# Evolution of the electronic structure of twisted bilayer $MoSe_2$

Sumanti Patra, Poonam Kumari, and Priya Mahadevan
*S. N. Bose National Centre for Basic Sciences, Block-JD, Salt Lake, Kolkata-700106, India*

(Received 14 May 2020; accepted 23 October 2020; published 12 November 2020)

In this work we examine the evolution of the electronic structure in twisted bilayers of $MoSe_2$, assuming the moiré potential to be a small perturbation to the untwisted limit. Its role in modifying the electronic structure is probed by mapping the calculated band structure for the moiré cell onto the primitive cell direction which represents the untwisted limit. At large twist angles such as 19.03°, we find that the moiré cell band structure is identical to the primitive cell one in the low-energy window. There are, however, significant deviations for small twist angles such as 3.48° which have large patches of high-symmetry regions of AA and AB′ stackings. These lead to enhanced interlayer hopping interaction strengths in some regions, and hence stronger perturbations leading to subband formation of the highest occupied band, which has a bandwidth of 19 meV and is found to be localized both in real space as well as in momentum space.

DOI: 10.1103/PhysRevB.102.205415

## I. INTRODUCTION

The ability to isolate a single monolayer [1,2] out of layered materials has led to artificially created structures built by placing these monolayers one on top of the other, sometimes with a small rotation of the upper layer with respect to the layer beneath. This artificial Legoland of structures created could involve similar monolayers [3–9] or dissimilar monolayers [10–13] with stacking bringing in an additional degree of freedom which is absent in the other popular techniques of growing materials layer by layer. The resulting unit cells could be much larger and even incommensurate in some instances in contrast to their few atom building blocks. One could also have physical properties very different from the constituent layers [14,15], which has led to a spurt of interest in these materials. This is especially spectacular because while the building blocks are uncorrelated materials, the twisted bilayers could have phenomena usually associated with the presence of strong electron-electron interactions [4–9].

These phenomena associated with twisted bilayer graphene were first suggested by the work of Bistritzer and MacDonald [16]. Considering a continuum model to describe the twisted structures, they calculated the electronic structure as a function of twist angle. At certain twist angles they found the Fermi velocity going to zero, implying flat bands and the possibility of the divergence of the electronic susceptibility which could drive some instabilities. These angles, referred to as magic angles, were identified as those at which superconductivity appeared [5,6]. More recently, they have also been observed in experiments on twisted bilayers of $WSe_2$ [7]. While there have been suggestions of flat bands in $MoS_2$ [17], a viewpoint for the existence of flat bands has been to associate them with the large moiré cells that one has, consequently leading to a small Brillouin zone because of zone folding.

In this work we reexamine the electronic structure of twisted bilayers of $MoSe_2$ considering certain angles that lead to large commensurate unit cells. The unit cells we generate contain $\simeq$1500 or more atoms while the primitive cell contains just six atoms. Consequently, one would expect no dispersional width for the bands here, with all bands folding back to a significantly small Brillouin zone. This has been the understanding of the formation of flat bands and the associated correlated electron physics that one finds. However, these structures have been generated by considering a bilayer with AA stacking and rotating the top layer with respect to the lower one. Consequently, they are not perfect supercells, but the fact that they are van der Waals materials implies a weak coupling between the layers which emerges from weak interlayer hopping interactions [18]. Even in the untwisted limit these lead to small modifications in the band structure of the bilayer with respect to the monolayer. For the twisted structures, in the limit of weak perturbation one expects the untwisted or unperturbed limit to be largely retained. Therefore a measure of the perturbation with respect to the untwisted limit could help us understand the modifications in the electronic structure. With this aim we unfolded the band structure onto the primitive cell direction. The effect of the perturbing moiré potential would be to scatter the electrons into a different momentum state connected by a reciprocal lattice vector. Two similarly sized moiré cells were considered for this purpose [19]. Surprisingly, one found that the low-lying electronic structure for the large twist angle of 19.03° was very similar to the unperturbed primitive cell results. This implied that the low-energy electronic structure for the large twist angles could be described by the unrotated limit, and most importantly flat bands were not a consequence of the large moiré cell involved. Considering a smaller angle of 3.48°, one found the emergence of bands which were localized in both real space as well as $k$ space, leading to split-off bands. These were not restricted to only this choice of twist

 ©2020 American Physical Society

angle, but were found for other angles also. Examining the origin of the flat band formation, we find that correlated bond disorder emerging from large patches where the interlayer interaction strengths are larger is responsible for the flat band formation. Including spin orbit interactions keeps the VBM at Γ for the twist angle of 3.48°, while that at the $K$ point is just 5 meV lower in energy. The presence of the split-off bands can explain the observation of successive semiconductor-metal-semiconductor transitions in twisted $WSe_2$ bilayers [7].

## II. METHODOLOGY

First-principle electronic structure calculations were carried out using density functional theory (DFT) within a Projector augmented plane wave method [20] as implemented in the Vienna *Ab initio* Simulation Package [21,22]. For the exchange-correlation functional we used Perdew-Burke-Ernzerhof potentials [23,24]. Lattice parameters were kept fixed at the experimental value of 3.289 Å [25], while the internal atomic positions were relaxed in each case through a total energy minimization which involved a minimization of the forces on each atom to a value less than $10^{-3}$ eV/Å. To minimize the interactions among the periodic images we introduced a vacuum of 20 Å along the $c$ direction, perpendicular to the plane of the bilayer for all structures. Weak van der Waals interactions were included using the DFT-D2 method of Grimme [26] to calculate the total energy in each case. A cutoff energy of 224 eV for the plane wave basis states is used for all the calculations. The electronic structure was solved self-consistently at the Γ point of the supercell. The numerical convergence of the results has been checked (see the Appendix).

The bilayers can have several arrangements of the second layer over the first, all leading to the same sized primitive cells. These lead to high-symmetry stackings for which we use the notation of Ref. [27]. The tear-and-stack technique used to make the bilayers allows the degree of freedom of forming structures that don't grow naturally. In our case we considered the atom on atom (AA stacking) for the bilayer and rotated the top layer with respect to the lower layer counterclockwise by an angle $\theta$. The choice of rotation angles were dictated by the computational effort involved. The calculated band structure for the large moiré cells was then projected onto the primitive cell symmetry directions by using a band unfolding technique as outlined in Ref. [28–30].

## III. RESULTS AND DISCUSSION

Before we examine the electronic structure of the twisted bilayers, we first consider the untwisted limit. Each monolayer (1H) has hexagonal planes of Se atoms on either side of a hexagonal plane of Mo atoms. As mentioned earlier, our starting point is a bilayer of $MoSe_2$ in which each atom of the upper layer sits on top of the same atom belonging to the lower layer. This leads to large repulsions between electrons belonging to the Se atoms in adjacent layers, leading to an increase in the interlayer separation to 3.79 Å in contrast to 3.19 Å found in the theoretically optimised calculations for the bulk-derived 2H structures. In spite of the variations in the interlayer separations, one finds that the shortest Se-Se bond

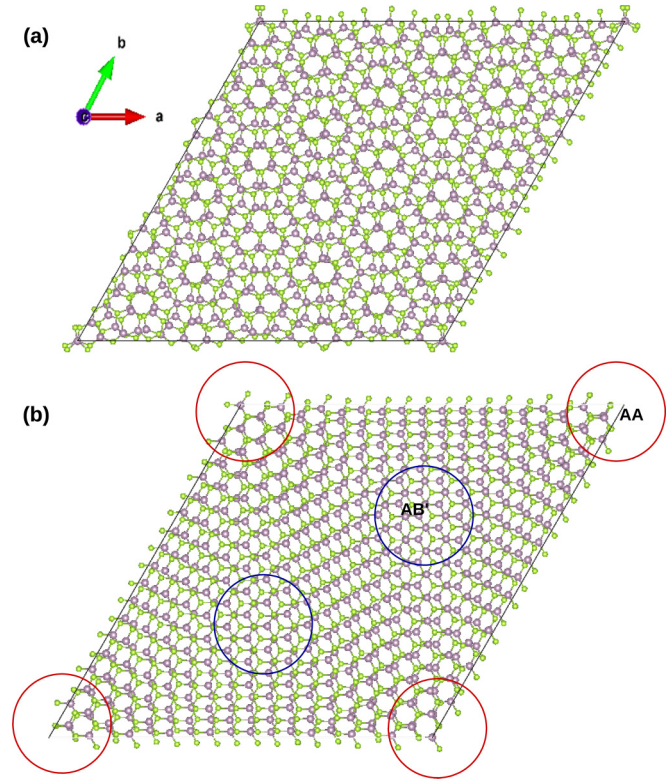


FIG. 1. Unit cell for twist angle (a) 19.03° and (b) 3.48°. The Mo/Se atoms are shown by violet/green spheres. Regions with high-symmetry stackings have been indicated.

length between atoms in the two layers is 3.79 Å. This is not very different from that found in the bulk-derived 2H stacking, where it is found to be 3.71 Å. It has been seen that the $d_{z^2}$ orbitals belonging to the two layers interact via the $p_z$ orbitals on Se, resulting in a bonding-antibonding splitting which is as large as 0.64 eV for bilayers of $MoSe_2$ at the Γ point for 2H stacking. As a combination of the in-plane $d_{x^2-y^2}/d_{xy}$ orbitals contribute at the $K$ point, the interlayer hopping interaction strength at $K$ is small between the two layers, leading to a splitting of just 0.094 eV there. Hence the monolayer band structure is hardly modified when one goes from monolayer to the bilayer [18]. This suggests that interlayer interactions may be treated as a perturbation. Varying the type of stacking leads to small changes in the electronic structure, with the general features discussed earlier present in all. While these stackings have a high symmetry associated with them which leads to small unit cells of six atoms, a small rotation of the upper layer with respect to the lower one leads to very large moiré cells. The unusual physics observed in the twisted bilayers has been associated with the large moiré cells. These lead to small Brillouin zones in reciprocal space. Consequently the length of vectors along the symmetry directions is short, and one expects flat bands.

We first considered a large twist angle of 19.03°, which led to a moiré cell that had 1482 atoms as shown in Fig. 1(a). While the rotation can lead to high-symmetry stackings in certain regions, for this large angle of rotation, we do not find any evidence of this. This leads to the interlayer separations showing small variations about a distance of 3.44 Å that

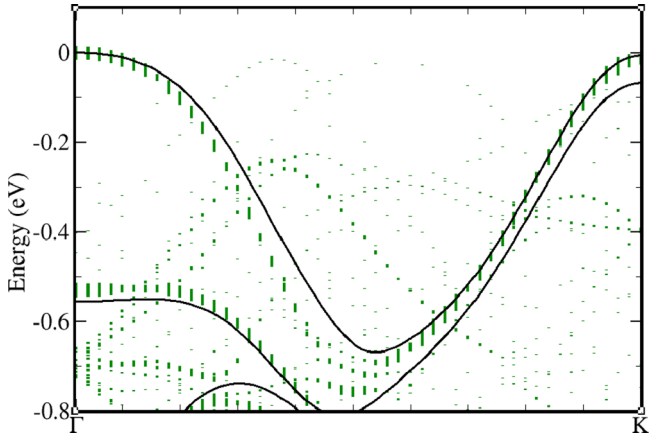


FIG. 2. Unfolded bandstructure for twist angle 19.03° projected along the primitive cell Γ to *K* direction. The thickness of each band represents its weight at that *k* point. The primitive cell band structure for AA stacking at an interlayer separation of 3.49 Å has been superposed for comparison.

we found earlier [29]. As each lattice vector in real space has a length of 51.69 Å, this leads to the reciprocal lattice vectors that are approximately a sixteenth of the length of the vectors for the primitive cell. The electronic structure for the supercell was calculated, and then in order to examine the extent of perturbation from the untwisted case, one found the projection at each *k* point along the primitive cell direction as shown in Fig. 2. The thickness of each band was chosen to be proportional to its weight at the *k* point. Indeed, if there was no perturbation as in a perfect supercell one would have 100% weight at each point and recover the primitive cell band structure. This is not the case, and the variations in the interlayer interaction strengths in each region lead to only a fraction of the weight in this direction. In order to examine the deviation, the primitive cell band structure for AA stacking calculated at the interlayer separation of 3.49 Å has also been plotted in black solid line. This represents the shortest Se-Se distance between atoms belonging to the two layers that one has for 19.03°. One finds hardly any deviation in the prominent low-energy bands comprising the valence band, suggesting that the moiré potential-induced perturbation is weak and the untwisted limit low-energy band structure is retained, with even the same magnitude of the bonding-antibonding splitting at Γ point, in contrast to what one finds for heterobilayers [31].

This behavior was observed at several large twist angles that were explored [29]. This raised the question whether this should be what is expected at all twist angles. In order to address this we considered a small twist angle where unusual deviations in the electronic structure were seen earlier in other transition metal dichalcogenides. The moiré cell that we have for a rotation angle of 3.48° had 1626 atoms as shown in Fig. 1(b). Here the length of each lattice vector in real space is 54.14 Å. In contrast to what we have for 19.03°, here we can identify regions which have AA as well as AB′ stackings. On carrying out a minimization of the forces on each atom, we find that analogous to the high-symmetry stacking involving only the primitive cell, one finds the interlayer separations

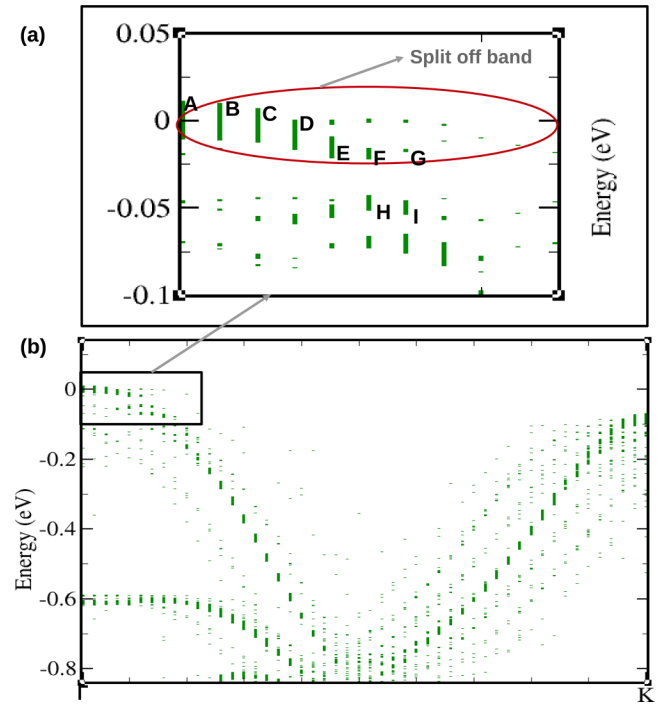


FIG. 3. Unfolded band structure for twist angles 3.48° along the primitive cell Γ to *K* direction. The thickness of each band represents it's weight at that *k* point. An expanded view of the band structure in panel (b) is shown in panel (a) with the points belonging to the band labeled A to I.

to have a minimum value of 3.19 Å in the regions with AB′ stacking and a maximum value 3.74 Å in the regions where the stacking is AA. This large variation in the interlayer separation is not found for the 19.03° twist. This is because for this large twist angle, the regions that one could identify with the high-symmetry stackings were small. Consequently any variations in the interlayer distance as seen for a twist of 3.48°would have a large strain energy cost associated with it. Hence we don't see it. However, when the regions are larger, the strain energy cost is overcome by the gain in overcoming Coulomb interactions between electrons in the two layers by an increased interlayer separation.

We then calculated the electronic structure for the moiré cell and the projection of each band along the primitive cell Γ-K direction as shown in Fig. 3. One finds the highest occupied band at Γ is energetically separated from the next highest band by 46 meV. In addition to being localized in real space (see the Appendix), one finds the band is localized in *k* space also. The band is identified to follow the path labeled A to G in Fig. 3(a) by following the character of the wave function, which should be continuous (see the Appendix). This places a dispersional width of 19 meV associated with the band. This behavior is not restricted to only this twist angle but is found at other small twist angles also. Similar subband formation has been seen in twisted bilayer graphene from angle-resolved photoemission experiments, split off from a strongly dispersing valence band [32]. Experiments on twisted bilayers of $WSe_2$ had found simultaneous semiconductor-metal-semiconductor transitions as holes were injected into the valence band [7]. The presence of subbands will capture

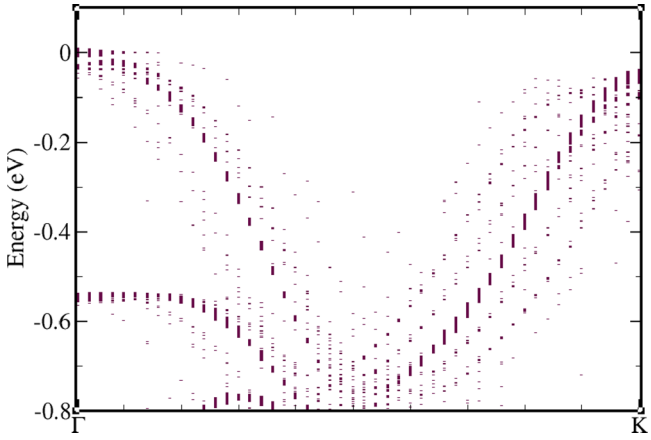


FIG. 4. Unfolded band structure for twist angle 3.48° along the primitive cell Γ to the $K$ direction. The thickness of each band represents its weight at that $k$ point. The interlayer separation has been kept fixed at 3.44 Å.

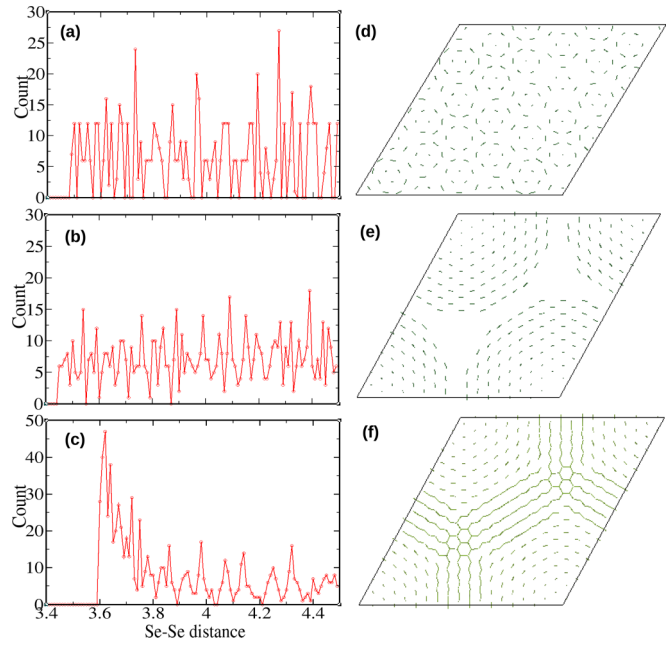


FIG. 5. Profile of Se-Se distances between the two layers for twist angles (a) 19.03°, (b) 3.48° at fixed interlayer separation, and (c) 3.48° (optimized structure). Spatial profile of interlayer Se-Se distances less than 3.8 Å for twist angles (d) 19.03°, (e) 3.48° at fixed interlayer separation, and (f) 3.48° (optimized structure).

these transitions found when there were two holes per moiré cell introduced by gating in twisted bilayers of $WSe_2$, and the picture may be valid for the entire $MX_2$ ($M$ = Mo, W; $X$ = S, Se, Te) family.

These results raise the question of the origin of the subband formation here and its absence at larger twist angles. As one difference that we had found in the structures was the large variations in the interlayer separations, we first examined if this was what was responsible. Earlier work for large twist angles had found that the interlayer separation was 3.44 Å. We therefore fixed the interlayer separation at this value and carried out a similar analysis of the moiré cell band structure. Here again we find the formation of a split-off band, shown in Fig. 4, indicating that the modulation in the interlayer separation is not responsible.

As discussed earlier [18], interlayer hopping interactions govern the changes in the electronic structure when an additional layer is added to a monolayer. The interlayer hopping interactions are primarily determined by the Se $p$ interactions of atoms on both layers. The distance ($r$) dependence of the hopping interaction strengths is given by an empirical law [33] and varies as $\frac{1}{r^{l+l'+1}}$, where $l$ and $l'$ are the angular momenta of the orbitals involved. So we went on to examine the variations in the interlayer Se-Se distances because these determine the relevant hopping interaction strengths. A distance profile giving the number of occurrences of pairs of Se atoms at a given distance has been given in Figs. 5(a)–5(c). One finds that the profile is quite similar for the 19.03° twist shown in Fig. 5(a) and the 3.48° twist with a fixed interlayer separation shown in Fig. 5(b). Hence the differences cannot emerge from variations in the Se-Se distance profile, which look quite similar in these two cases. The distance profile has also been given for the 3.48° twist for which the atomic positions were relaxed to the minimum energy position. One finds the distance profile to be drastically different with the shortest interlayer Se-Se distance being at least 3.6 Å in contrast to the other cases. Additionally the number of Se-Se bonds with distances less than 3.8 Å is significantly higher here. As the distance profile cannot explain the differences in electronic structure, we went on to examine the spatial distribution of the Se atoms in the cell with Se-Se distances less than 3.8 Å. This would give us an idea of where the perturbation to the monolayer band structure from the interlayer hopping interactions would be the strongest. This distribution was found to be random for the 19.03° twist, while both cases for the 3.48° twist revealed similarities. One found a concentration of these bond lengths in some regions, although the distributions were not identical. This implied that a concentrated disorder arising from interlayer hopping interaction strengths was responsible for the subband formation. This arose from the large regions where we had the high-symmetry stackings which result in large perturbations to the electronic structure leading to subband formation. This should be present at other small twist angles also (see the Appendix). As discussed earlier, for larger twist angles the regions of high-symmetry stackings are too small, and hence the perturbation is weaker with no subband formation.

The above results are for calculations without spin-orbit interactions being considered. On including them, we found that the valence band maximum remained at Γ point. Earlier work [34] has shown strain to be a handle to shift the valence band maximum from Γ to $K$ in transition metal dichalcogenides. We therefore explored the nature of the highest occupied band at the $K$ point also. This is just 5 meV lower in energy than the valence band maximum at Γ. We find subband formation here also; however, here the subbands are not separated from each other as seen at Γ. This could be because of a weaker interlayer coupling strength at $K$.

## IV. CONCLUSION

In this work we have examined the perturbation in the electronic structure of twisted bilayers of $MoSe_2$ arising from spatially varying interlayer hopping interactions. Large twist angles lead to the low-lying electronic structure that is very similar to the primitive cell limit. At small twist angles the structures reveal patches with high-symmetry AA and AB′ stackings. These lead to regions where the interlayer hopping interaction strengths are enhanced and consequently a larger perturbation of the electronic structure. One finds a split-off band at the top of the valence band which has a dispersional width of 19 meV. This is localized in both real space and $k$ space and is separated from the next band at the Γ point by 46 meV. These features in the electronic structure could explain the unusual electronic structure seen in $WSe_2$ and hint at similar behavior in the entire family of Mo- and W-based dichalcogenides.

## ACKNOWLEDGMENTS

We thank DST Nanomission for support through the project DST/NM/NS/2018/18.

## APPENDIX

### A. Charge density of valence band maximum

The charge density shown in Fig. 6 is for the valence band maximum located at Γ of the band structure shown in Fig. 3.

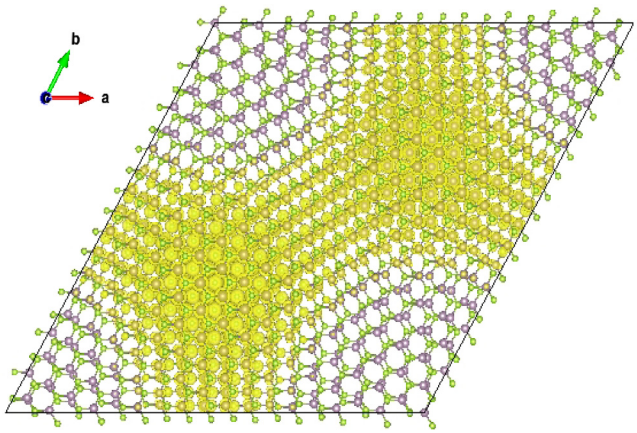


FIG. 6. Charge density associated with the valence band maximum at Γ for twist angle 3.48°.

### B. Character of states labeled in the unfolded band structure for twist angle 3.48°

Integrated charge density within a sphere of radius 1.262 Å (half the Mo-Se bond length) around one Mo atom for points A to I labeled in Fig. 3, have been shown in Table I. The character is found to change gradually along the path A to G, while it is drastically different for points H and I labeled in Fig. 3.

TABLE I. Integrated charge density over a sphere of radius 1.262 Å (half the Mo-Se bond length) around one Mo atom for points A to I in Fig. 3. The normalization is arbitrary.

| Labeled point | Integrated charge density over a sphere around one Mo atom |
|---|---|
| A | 58.639 |
| B | 60.185 |
| C | 66.331 |
| D | 67.727 |
| E | 69.181 |
| F | 81.844 |
| G | 73.195 |
| H | 5.021 |
| I | 5.012 |

### C. Unfolded band structure for twist angle 5.36°

Unfolded band structure for another small twist angle (5.36°) has been shown in Fig. 7.

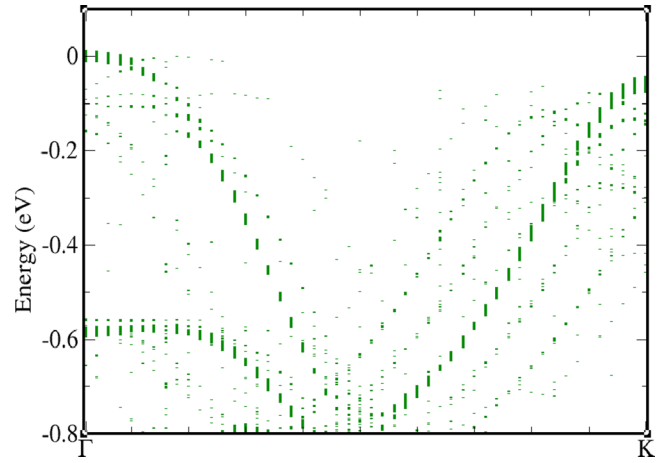


FIG. 7. Unfolded band structure for twist angle 5.36° along Γ to $K$ of the primitive cell direction.

### D. Density of states:

Density of states (DOS) as a function of energy is shown (Figs. 8 and 9) for both the twist angle 19.03°and 3.48°. In each case, a $4 \times 4 \times 1$ $k$ mesh is used for the calculation.

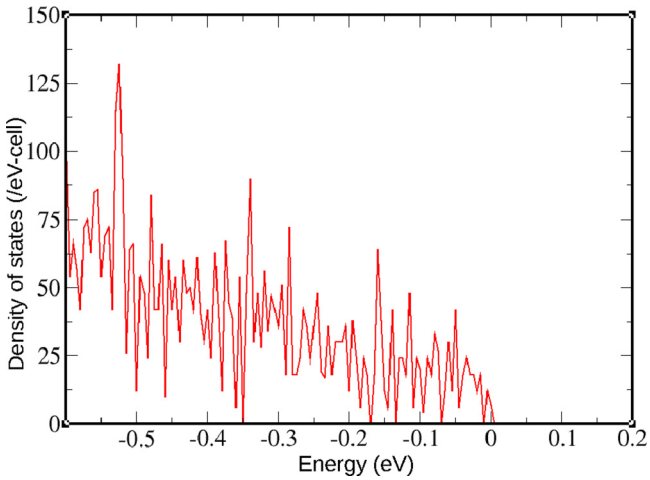


FIG. 8. Density of states as a function of energy for twist angle 19.03°.

### E. Convergence tests:

The convergence test for the vacuum as well as the cutoff energy for the plane wave basis set used in the calculations are shown in Figs. 10 and 11. The convergence of the eigenvalues as a function of the k points mesh used in the ab initio calculation is given in Table II.

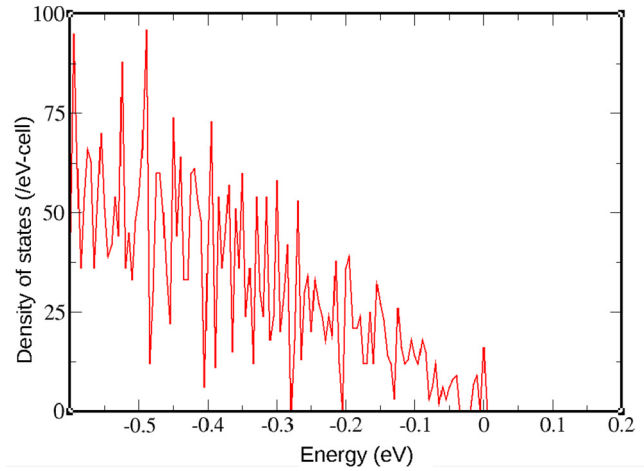


FIG. 9. Density of states as a function of energy for twist angle 3.48°.

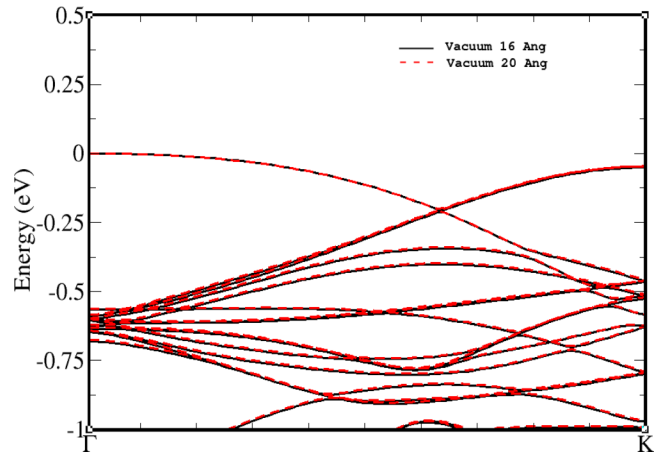


FIG. 10. Superposed band structure (along Γ to *K* of supercell) with vacuum 16 Å and 20 Å for twist angle 21.8°.

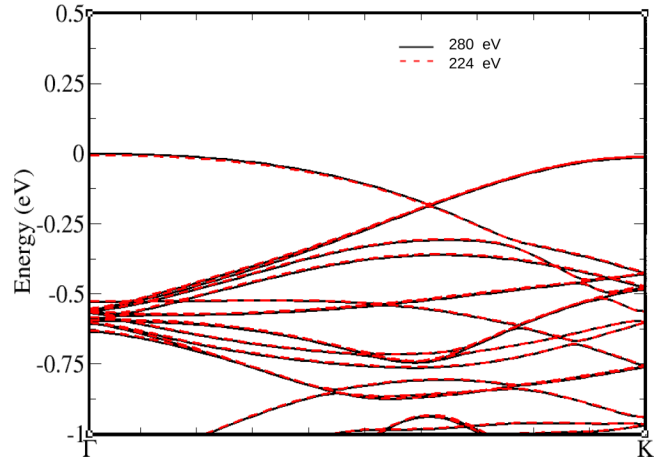


FIG. 11. Superposed band structure (along Γ to *K* of supercell) with cutoff energies of 224 eV and 280 eV for twist angle 21.8°.

TABLE II. Energies of the top few valence bands starting from the valence band maximum for twist angle 3.48°shown for a *k*-point mesh of 4 × 4 × 1 and 1 × 1 × 1 to compare the energies.

| Eigenvalue (eV) for *k*-point mesh 4 × 4 × 1 | Eigenvalue (eV) for *k*-point mesh 1 × 1 × 1 |
|---|---|
| −0.9453 | −0.9455 |
| −0.9649 | −0.9651 |
| −0.9919 | −0.9921 |
| −0.9922 | −0.9923 |
| −1.0149 | −1.0149 |
| −1.0150 | −1.0150 |
| −1.0468 | −1.0467 |
| −1.0468 | −1.0467 |
| −1.0588 | −1.0588 |
| −1.0623 | −1.0622 |

[1] K. S. Novoselov, A. K. Geim, S. V. Morozov, D. Jiang, Y. Zhang, S. V. Dubonos, I. V. Grigorieva, and A. A. Firsov, Science **306**, 666 (2004).

[2] K. S. Novoselov, A. K. Geim, S. V. Morozov, D. Jiang, M. I. Katsnelson, I. V. Grigorieva, S. V. Dubonos, and A. A. Firsov, Nature (London) **438**, 197 (2005).

[3] P.-C. Yeh, W. Jin, N. Zaki, J. Kunstmann, D. Chenet, G. Arefe, J. T. Sadowski, J. I. Dadap, P. Sutter, J. Hone, and J. R. M. Osgood, Nano Lett. **16**, 953 (2016).

[4] Y. Jiang, X. Lai, K. Watanabe, T. Taniguchi, K. Haule, J. Mao, and Eva Y. Andrei, Nature (London) **573**, 91 (2019).

[5] Y. Cao, V. Fatemi, S. Fang, K. Watanabe, T. Taniguchi, E. Kaxiras, and P. Jarillo-Herrero, Nature (London) **556**, 43 (2018).

[6] Y. Cao, V. Fatemi, A. Demir, S. Fang, Spencer L. Tomarken, J. Y. Luo, J. D. Sanchez-Yamagishi, K. Watanabe, T. Taniguchi *et al.*, Nature (London) **556**, 80 (2018).

[7] L. Wang, E.-M. Shih, A. Ghiotto, L. Xian, D. A. Rhodes, C. Tan, M. Claassen, D. M. Kennes, Y. Bai, B. Kim *et al.*, Nat. Mater. **19**, 861 (2020).

[8] P. S. Mahapatra, K. Sarkar, H. R. Krishnamurthy, S. Mukerjee, and A. Ghosh, Nano Lett. **17**, 6822 (2017).

[9] P. C. Adak, S. Sinha, U. Ghorai, L. D. V. Sangani, K. Watanabe, T. Taniguchi, R. Sensarma, and M. M. Deshmukh, Phys. Rev. B **101**, 125428 (2020).

[10] Z. Wang, D.-K. Ki, H. Chen, H. Berger, A. H. MacDonald, and A. F. Morpurgo, Nat. Commun. **6**, 8339 (2015).

[11] P. Rivera, J. R. Schaibley, A. M. Jones, and J. S. Ross, Nat. Commun. **6**, 6242 (2015).

[12] C. Jin, E. C. Regan, A. Yan, M. I. B. Utama, D. Wang, S. Zhao, Y. Qin, S. Yang, Z. Zheng, S. Shi *et al.*, Nature (London) **567**, 76 (2019).

[13] R. Ribeiro-Palau, C. Zhang, K. Watanabe, T. Taniguchi, J. Hone, and C. R. Dean, Science **361**, 690 (2018).

[14] L. A. Gonzalez-Arraga, J. L. Lado, F. Guinea, and P. San-Jose, Phys. Rev. Lett. **119**, 107201 (2017).

[15] Y. Cao, J. Y. Luo, V. Fatemi, S. Fang, J. D. Sanchez-Yamagishi, K. Watanabe, T. Taniguchi, E. Kaxiras, and P. Jarillo-Herrero, Phys. Rev. Lett. **117**, 116804 (2016).

[16] R. Bistritzer and A. H. MacDonald, Proc. Natl. Acad. Sci. USA **108**, 12233 (2011).

[17] M. H. Naik and M. Jain, Phys. Rev. Lett. **121**, 266401 (2018).

[18] S. K. Pandey, R. Das, and P. Mahadevan, ACS Omega **5**, 15169 (2020).

[19] It is believed that large twist angles lead to small unit cell sizes, but this is not the case.

[20] P. E. Blöchl, Phys. Rev. B **50**, 17953 (1994).

[21] G. Kresse and J. Hafner, Phys. Rev. B **47**, 558 (1993).

[22] G. Kresse and J. Hafner, Phys. Rev. B **49**, 14251 (1994).

[23] J. P. Perdew, K. Burke, and M. Ernzerhof, Phys. Rev. Lett. **77**, 3865 (1996).

[24] R. Elmer, M. Berg, L. Carlen, B. Jakobsson, B. Noren, A. Oskarsson, G. Ericsson, J. Julien, T. F. Thorsteinsen, M. Guttormsen *et al.*, Phys. Rev. Lett. **78**, 1396(E) (1997).

[25] K. D. Bronsema, J. L. de Boer, and F. Jellinek, Z. Anorg. Alg. Chem. **540/541**, 15 (1986).

[26] S. Grimme, J. Comput. Chem. **27**, 1787 (2006).

[27] J. He, K. Hummer, and C. Franchini, Phys. Rev. B **89**, 075409 (2014).

[28] V. Popescu and A. Zunger, Phys. Rev. B **85**, 085201 (2012).

[29] P. Kumari, J. Chatterjee, and P. Mahadevan, Phys. Rev. B **101**, 045432 (2020).

[30] Y. Tan, F. Chen, and A. W. Ghosh, arXiv:1606.01858 (2016).

[31] G. C. Constantinescu and Ni. D. M. Hine, Phys. Rev. B **91**, 195416 (2015).

[32] M. I. B. Utama, R. J. Koch, K. Lee, N. Leconte, H. Li, S. Zhao, L. Jiang, J. Zhu, K. Watanabe, T. Taniguchi *et al.*, Nat. Phys. (2020); S. Lisi, X. Lu, T. Benschop, T. A. de Jong, P. Stepanov, J. R. Duran, F. Margot, I. Cucchi, E. Cappelli, A. Hunter *et al.*, arXiv:2002.02289 (2020).

[33] W. A. Harrison, *Electronic Structure and the Properties of Solids* (Dover, New York, 1980)

[34] R. Das, B. Rakshit, S. Debnath, and P. Mahadevan, Phys. Rev. B **89**, 115201 (2014)